Fast Numerical Simulation for Full Bore Rupture of Pressurized Pipelines

Haroun Mahgerefteh, Pratik Saha, and Ioannis G. Economou
Dept. of Chemical Engineering, University College London, London WC1E 7JE, United Kingdom

An efficient numerical simulation (CNGS-MOC), based on the method of characteristics for simulating full bore rupture of long pipelines containing two-phase hydrocarbons, was developed. The use of curved characteristics, in conjunction with a compound nested grid system, as well as a fast mathematical algorithm, lead to a significant reduction of CPU time, while improving accuracy. The model is validated extensively against field data including those obtained during the Piper Alpha tragedy, as well as the Isle of Grain depressurization tests. Its predictions are compared with those based on other mathematical models including PLAC, META-HEM, MSM-CS, as well as BLOWDOWN. Both CNGS-MOC and META-HEM produce reasonably accurate predictions with the remaining models assessed performing relatively poorly.

Introduction

The most common way of exporting oil and gas from offshore installations is through long pipelines. The combination of the high pressure needed to induce flow, as well as the massive amount of inventory present in the pipeline, pose a risk of full bore rupture (FBR), which, in the event of occurring, can lead to one of the most catastrophic types of accidents possible in the offshore industry. During the Piper Alpha tragedy (Cullen, 1990), for example, the rupture of the three gas export pipelines, although not the primary cause of the accident, resulted in the major escalation of the incident and the eventual collapse of the platform. There have also been several other documented cases relating to FBR, which have resulted in numerous loss of life and significant damage to the environment (Bond, 1996).

Consequently, an important part of the safety assessment case (HMSO, 1989) for all offshore platforms utilizing subsea pipelines greater than 40 cm in diameter is the prediction of the amount of inventory released and its variation with time in the event of FBR. Such information has a direct impact on almost every safety aspect of the platform including the survival time of the temporary safe refuge.

Another area of concern is during controlled release or blowdown. In such cases, prior estimations of the resulting temperature drops in the fluid and the pipeline are of primary importance in order to avoid pipeline brittle fracture or the formation of solid hydrates, which can in turn lead to blockage.

The depressurization process is not amenable to simple analysis due to its highly transient unsteady-state nature. Despite this, in recent years, several workers have proposed empirical correlations based on experimental data (Weiss et al., 1988). These are, however, very limited in the range of applicability and particularly inappropriate for pipelines containing two-phase or condensable mixtures. Also, apart from providing an estimate of the release rate with time, no other information on the variation of the fluid dynamics within the pipeline during depressurization is provided. The critical role of this type of data is already demonstrated in governing the dynamic response, as well as the integrity of emergency shutdown valves following FBR of gas pipelines (Mahgerefteh et al., 1997, 1998).

The partial differential equations pertaining to conservation of mass, momentum, and energy for an element of the fluid medium within the pipeline constitute a system of essentially Euler equations. These incorporate a stiff source term due to the friction in the momentum equation. Heat-transfer effects, on the other hand, are taken into account in the energy equation. These non-negligible nonisentropic effects together with the choked flow boundary condition render modeling of depressurization as a result of FBR different from flow in a shock tube (Lyczkowski et al., 1978 a,b).

Correspondence concerning this article should be addressed to H. Mahgerefteh.
Current address of I. G. Economou: Molecular Modelling of Materials Lab., Institute of Physical Chemistry, National Research Centre for Physical Sciences "Demokritos," GR-15310 Aghia Paraskevi Attikis, Greece.

The inviscid part of the conservation equations can be shown to be hyperbolic (Zucrow and Hoffmann, 1976) with three real eigenvalues. The resulting Euler equations can be solved using a variety of numerical techniques with varying degrees of success. Previous attempts include a finite difference method (FDM) (Chen et al., 1993, 1995a,b; Bendiksen et al., 1991), a finite-element method (FEM) (Lang, 1991; Bisgaard et al., 1987) and the method of characteristics (MOC) (Chen et al., 1992; Flatt, 1986; Olorunmaiye and Imide, 1993). As all of these techniques in essence involve the numerical discretization of the pipeline into a large number of elements, a solution invariably requires very long CPU time (40 days on a 300 MHz Pentium II processor can be typical). This problem is exceptionally acute in the case of MOC particularly when simulating FBR of long pipelines (> 100 km), typical of North Sea operations.

In this study, the MOC is adopted to simulate FBR or blowdown of long pipelines containing condensable or two-phase hydrocarbon mixtures. This technique is employed as opposed to FDM and FEM, as both have difficulty in handling the choking condition at the ruptured end. The MOC handles choked flow intrinsically via the Mach line characteristics. Moreover, MOC is considered to be more accurate than FDM, as it is based on the characteristics of wave propagation. Hence, numerical diffusion associated with a finite difference approximation of partial derivatives is avoided (Chen et al., 1992). The effects of valve closure during emergency shutdown on the fluid dynamics within the pipeline are simply and conveniently handled by specifying the appropriate boundary conditions across the valve at selected time and space grids. The number of iterations involved are dramatically reduced in MOC by setting up and solving a system of simultaneous equations. The above together with the use of second-order or curved characteristics, and a nested grid system, result in a significant reduction in CPU time.

This procedure allowed for the first time extensive evaluation of the performance of MOC in simulating FBR throughout the discharge process by comparison with field data, as well as other solution techniques including META-HEM (Chen et al., 1995a,b; Chen, 1993), MSM-CS (Chen et al., 1995a,b; Chen 1993), BLOWDOWN (Richardson and Saville 1991) and PLAC (Hall et al., 1993). The field data were from pipeline depressurization tests carried out in the Isle of Grain (Richardson and Saville, 1996), as well as those recorded during the night of the Piper Alpha tragedy (Chen, 1993). The simulations were performed on the basis of an homogeneous equilibrium model (HEM) in which all phases are assumed to be at thermal and phase equilibrium. Comparison with experimental data (Picard and Bishnoi, 1989; Chen, 1993; Chen et al., 1995) has shown that this assumption is applicable to FBR of long (>100 m) pipelines.

Model Development

Characteristic and compatibility equations

For one-dimensional (1-D) multiphase homogeneous flow where thermodynamic and phase equilibrium exist simultaneously and that fluid/structure interactions (Lawooij and Tijsselling, 1990; Stittgen and Zielke, 1990) are negligible, the continuity, momentum, and energy conservation equations for an element of the fluid within the pipeline are respectively given by (Chen et al., 1993)

$$\rho_t + \rho u_x + u\rho_x = 0$$
$$\rho u_t + \rho u u_x + P_x - \beta = 0$$
$$P_t + uP_x - a^2(\rho_t + u\rho_x) - \psi = 0 \qquad (1)$$

where ρ, u, P, β, and a are the density, velocity, pressure, friction force term, and acoustic velocity of the fluid, respectively. Subscripts t and x denote property derivative with respect to time and space (in the x-direction), respectively. Furthermore, ψ is the nonisentropic term incorporating heat transfer and frictional effects given by

$$\psi = \varphi\frac{q_h - u\beta}{\rho T} \qquad (2)$$

where q_h is the heat transfer from the pipe wall to the fluid. The thermodynamic function φ is given by

$$\varphi = \left(\frac{\partial P}{\partial s}\right)_\rho \qquad (3)$$

The MOC involves the replacement of the three conservation equations by the following characteristic and compatibility equations

$$\left(\frac{dt}{dx}\right)_p = \frac{1}{u} \qquad \text{(path line characteristic)} \qquad (4)$$

$$\left(\frac{dt}{dx}\right)_\pm = \frac{1}{u \pm a} \qquad \text{(Mach line characteristics)} \qquad (5)$$

The characteristic Eqs. 4 and 5 stipulate the way in which information is propagated through a flow field. In regions where fluid properties change dramatically, in a nonlinear manner, the characteristics are curved (Flatt, 1985). This is usually the case for two-phase mixtures or condensable gases. It is assumed that straight line characteristics can lead to significant global errors. Figure 1 shows the characteristics curves.

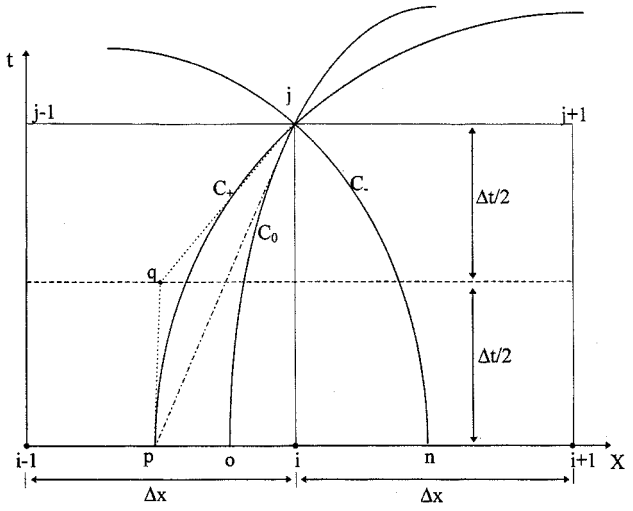

Figure 1. Curved (second-order) characteristics.

The pathline compatibility C_o is

$$dP - a^2 d\rho = \frac{\psi}{u} dx = \psi dt \tag{6}$$

The positive C_+ and negative C_- compatibility equations can be written as

$$d_\pm P \pm \rho a d_\pm u = [\psi \pm a\beta] dt \tag{7}$$

The values of P, ρ, u, and a as a function of time and distance along the pipeline (say, points, p, o and n, in Figure 1) may be obtained by the inverse marching method of characteristics. This involves dividing the pipeline into a large number of distance (Δx) and time elements (Δt), expressing the compatibility equations in finite difference form, and solving them at the intersection of the characteristics curves with the spatial axis (points p, o, n, and j). The loci of points, p, o, n, and j are found by accounting for the curvature of the characteristics by considering them as arcs of parabolas and making use of the geometrical fact that the tangents at point j and p meet halfway along the time axis at point q. The previous time line properties are calculated directly from solution of quadratic interpolation formulas for spatial discretization. The effect of accounting for curved characteristics as opposed to the extensively used linear approximation (Chen et al., 1992; Flatt, 1986; Picard and Bishnoi, 1989) on the CPU time required and on the accuracy is quantified later. Numerical stability requires the fulfillment of the Courant-Friedrich-Lewy Criterion (Courant et al., 1926; Zucrow and Hoffman, 1976) given by

$$\Delta t = \frac{\Delta x}{(|u + a|_{\max})_{t=0}} \tag{8}$$

The coupling of the flow equations using a compound nested grid system (CNGS, see later) together with the thermodynamic and phase equilibrium equations based on HEM form the basis of the CNGS employed in this study. Before the calculation procedure for this model is presented, the important thermophysical and hydrodynamic constitutive relations are to be addressed. All hydrodynamic constitutive relations pertaining to momentum exchange between two phases are nonexistent as we assume HEM.

Thermophysical properties

Phase equilibrium calculations are performed with the widely used Peng-Robinson equation-of-state EoS (Peng and Robinson, 1976), which is particularly useful for handling multicomponent hydrocarbon mixtures. The number and the appropriate fluid phase(s) present are obtained using the stability test based on the Gibbs tangent plane criterion developed by Michelsen (1982a,b, 1987). For unstable systems, the technique also provides the composition of a new phase which can be split off to decrease the Gibbs energy of the mixture.

Pseudo-fluid properties for mixtures are calculated on the basis of pure liquid and gas properties obtained from the EoS. For example, the mixture density ρ is given by

$$\rho = \frac{\rho_g \rho_l}{\rho_g(1 + \chi) + \rho_l \chi} \tag{9}$$

where the subscripts g and l denote the gas and liquid phase, respectively, and χ refers to the mass of vapor per unit mass of bulk fluid. The speed of sound a and φ, for real multicomponent multiphase fluids, are written as (Groves et al., 1978; Picard and Bishnoi, 1988) follows. For the case of single phase mixtures, it is

$$a^2 = \frac{\gamma}{k\rho} \tag{10}$$

$$\varphi = \frac{\rho \xi T a^2}{c_p} \tag{11}$$

where γ is the ratio of specific heats, and k and ξ are the isothermal and isobaric coefficients of volumetric expansion, respectively, and c_p is the specific heat capacity at constant pressure. All these parameters are easily obtained from the Peng-Robinson EoS. For two-phase flows, the analytical determination of γ and c_p becomes complex. Hence, the parameters a and φ are evaluated numerically at a given temperature and pressure. The sound velocity at a certain temperature T and pressure P can be expressed as

$$a^2 = \frac{\Delta P}{\rho(T, P)_s - \rho(T^*, P - \Delta P)_s} \tag{12}$$

where the subscript s denotes a constant entropy condition.

To solve for T^*, a Newton-Raphson iteration is performed where the objective function is written as

$$\omega^{(n)} = s(T, P) - s(T^{*(n)}, P - \Delta P) \tag{13}$$

where superscript (n) denotes the iteration level.

The numerical expression for the parameter φ can be obtained from the expression

$$\varphi = \left(\frac{\Delta P}{\Delta s}\right)_\rho = \rho^2 \left(\frac{\Delta T}{\Delta \rho}\right)_s \tag{14}$$

The latter equation is solved numerically by performing an isentropic flash calculation using Eq. 12.

Frictional force effects

At the fluid-wall interface, the presence of the viscous drag force can be modeled as a linear combination of unsteady and steady wall drag or friction (Chen, 1993). From an earlier review (Saha, 1997), it seems that there is still some uncertainty in the accurate prediction of an unsteady friction factor in rough pipes where highly turbulent flows prevail. Moreover, from the few studies performed to date (Zucrow and Hoffman, 1976; Wood and Funk, 1970), the effect of the unsteady component in wall shear stress calculations seems to diminish in magnitude as the turbulence of flow increases. In the absence of any theoretically and experimentally justified transient turbulent friction calculation for rough pipes, it was decided to ignore this component in the model proposed in the present study.

The steady flow friction factor was estimated using the Moody (Massey, 1983) approximation to Colebrooke's equa-

tion. It is the most accurate expression available, representing results within 5% of experimental data, and is given by

$$f_w = 0.001375\left[1+\left(20{,}000\frac{\epsilon}{D}+\frac{10^6}{Re}\right)^{1/3}\right] \tag{15}$$

which is valid for $Re \geq 2{,}000$.

For $Re \leq 2{,}000$, the following well established laminar flow correlation is employed

$$f_w = \frac{16}{Re} \tag{16}$$

Two-phase mixtures are simply handled by replacing single-phase properties by two-phase mixture properties. Therefore, for a two-phase mixture,

$$\beta = -2\frac{f_{wm}}{D}\rho_m u|u| \tag{17}$$

where f_{wm} is the two-phase mixture friction factor and can be determined either from Eq. 15 or 16.

The mixture viscosity is given by

$$\frac{1}{\mu_m} = \frac{\chi}{\mu_g}+\frac{(1-\chi)}{\mu_l} \tag{18}$$

The gas and liquid viscosities are calculated according to the Ely and Hanley scheme for nonpolar gaseous mixtures, and the Dymond and Assael scheme for liquid mixtures (Massey, 1983).

Numerical discretization of the pipeline

The grid structure for numerical discretization of the pipeline length is based on a Compound Nested Grid System (CNGS) described in earlier publications (Mahgerefteh et al., 1997, 1998). Briefly, it involves the use of increasingly finer grids near the rupture plane where the transients are most rapid. This procedure results in a significant reduction of CPU time as coarser grids can in turn be used at locations away from the rupture plane. Since the smaller grids are geometrically similar, and contained within the large *normal* mesh, a consistent Courant number (Courant et al., 1926) is maintained throughout the discharge process and numerical instability is avoided.

Initial condition

Steady-State Flow Prior to Rupture. It is assumed that the flow in the pipeline prior to rupture can be taken to be isothermal steady state. It can be shown that the corresponding pressure drop across an element Δx is given by

$$P_i = P_{i-1}+\frac{\beta_{i-1}}{\left[1-\dfrac{u^2}{ZRT}\right]_{i-1}}\Delta x \tag{19}$$

The change in velocity as a result of this pressure drop is

$$u_i = u_{i-1}\left(1-\frac{\Delta P}{(\rho ZRT)_{i-1}}\right) \tag{20}$$

where the subscript i denotes the grid points at which the fluid conditions are being calculated, and $i-1$ refers to the fluid conditions at the previous grid point.

Rupture Plane Calculation at $t = 0$. For a change in pressure from initial pressure P_{in} to a given pressure P following FBR, the fluid discharge velocity at the rupture plane is given by

$$u = -\int_{P_{\text{in}}}^{P}\frac{dP}{\rho a} \tag{21}$$

For a condensable gas mixture, the thermodynamic relationship between ρ, a, and P becomes highly nonlinear and Eq. 21 can only be solved numerically. Expressing this equation in finite difference form results in

$$u_{r+1} = u_r - \left[\frac{P_{r+1}-P_r}{(\rho a)_r}\right] \tag{22}$$

where r shows the current level of decompression and $r+1$ denotes the new level resulting from an incremental decompression step. In this study the new pressure is taken as

$$P_{r+1} = 0.95P_r \tag{23}$$

The calculation procedure for the boundary condition at the rupture plane at $t = 0$ assuming isentropic expansion is as follows:

- Start the decompression process at the initial pressure P_{in} and temperature T_{in} and calculate the bulk density and speed of sound by performing an isothermal flash (the entropy is kept constant throughout the decompression process).
- Calculate the new fluid pressure and velocity using Eqs. 23 and 22, respectively. Perform an isentropic pressure-entropy flash based on the initial entropy, and the new pressure to obtain a new density and speed of sound.
- Compare the new speed of sound a_{r+1} and velocity u_{r+1}. If velocity is less than speed of sound, then repeat calculation until $u_{r+1} = a_{r+1}$, when the fluid conditions at the rupture plane are known based on an isentropic decompression.

Interior Point Calculation at $t > 0$. The methodology for the calculation of the conditions at a solution point (such as point j in Figure 1) was described earlier. Calculation of the corresponding temperature involves the solution of the following equation

$$\rho_j - \rho\left(T_j^r, P_j\right) = 0 \tag{24}$$

based on an iterative numerical scheme. The subscript j denotes conditions at the solution point (see Figure 1), and the superscript r is related to the unknown temperature. The solution of Eq. 24 becomes a root finding problem where a temperature is sought to match the density obtained from the compatibility equations to that calculated from an isothermal

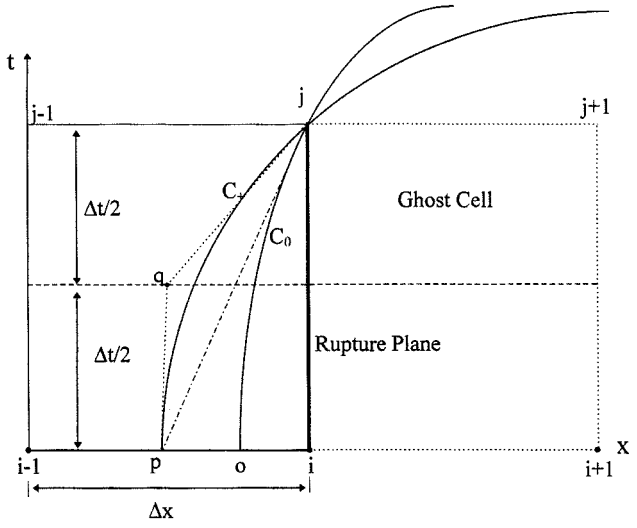

Figure 2. Boundary cell layout.

pressure-temperature flash. For this purpose, the method of Brent (Press et al., 1994) was employed according to which the bracketing of the root is performed, and, for our calculations, it produces rapid convergence. Once the temperature is obtained at the solution point, the speed of sound and the parameter φ are found by a flash calculation. The above steps are repeated until convergence is achieved for the dependent variables P, ρ and u.

Rupture Plane Calculation at $t > 0$. The methodology used for the curved characteristics in the boundary cell involves the addition of an extra ghost cell adjacent to the boundary cell as shown in Figure 2. This permits quadratic interpolation for points p and o. The conditions at the node $i+1$ are the same as at the node i, that is

$$\Omega_{i+1} = \Omega_i \tag{25}$$

where

$$\Omega = P,\ u,\ \rho,\ T, \text{ or } a.$$

The rest of the calculations are exactly the same as those for the interior point with the exception that simultaneous solution of the positive and pathline compatibility equations is not possible, since no algebraic relationship exists for the speed of sound of a two-phase mixture. The negative or left running characteristic at the rupture plane will be vertical [the gradient, $1/(u-\mathrm{a})$ is infinity], and, hence, perpendicular to the x-axis, as shown in Figure 2. Since the negative Mach line is vertical, the conditions at the previous time level x_i are already known, so that the negative compatibility equation expressed in a finite difference form becomes

$$P_j - P_i - \frac{1}{2}\left((\rho a)_i + (\rho a)_j\right)(u_j - u_i) = \frac{1}{2}\left((\psi - a\beta)_i + (\psi - a\beta)_j\right)(t_j - t_i) \tag{26}$$

This compatibility equation can be solved together with the pathline and positive compatibility equations given by Eqs. 6 and 7, respectively. The calculations of bulk density and speed of sound are obtained from Eqs. 9 and 10 or 12, respectively.

Calculation at the Boundary between Grids of Different Size. The use of a nested grid system creates boundaries between different size grids. To deal with these regions, a direct solution technique has been developed which is particularly suited to highly transient two-phase flows. In Figure 3, this technique is illustrated for the calculation at solution point $j+4$. The path line compatibility is given by

$$\lambda_o = \frac{d_o t}{d_o x} = \frac{1}{u_o} = \frac{4\Delta t_1}{x_i - x_o} \Rightarrow x_o = x_i - 4\Delta t_1 u_o \tag{27}$$

The positive and negative characteristics are respectively given by

$$\frac{d_+ t}{d_+ x} = \frac{1}{u_p + a_p} = \frac{4\Delta t_1}{x_i - x_p} \Rightarrow x_p = x_i - 4\Delta t_1(u_p + a_p) \tag{28}$$

$$\frac{d_- t}{d_- x} = \frac{1}{u_n - a_n} = \frac{\Delta t_1}{x_i - x_n} \Rightarrow x_n = x_i - \Delta t_1(u_n - a_n) \tag{29}$$

Using Eqs. 28–29 and linear interpolation, the simultaneous equations for the solution at points u_p and a_p are

$$u_p\left(1 + \frac{u_i - u_{i-1}}{\Delta x_2} 4\Delta t_1\right) + \frac{u_i - u_{i-1}}{\Delta x_2} 4\Delta t_1 a_p = u_i \tag{30}$$

$$a_p\left(1 + \frac{a_i - a_{i-1}}{\Delta x_2} 4\Delta t_1\right) + \frac{a_i - a_{i-1}}{\Delta x_2} 4\Delta t_1 u_p = a_i \tag{31}$$

Similarly, a 2×2 system of equations can be set up for obtaining u_n and a_n. These are given by

$$u_n\left(1 + \frac{u_{i+1} - u_i}{\Delta x_1}\Delta t_1\right) - \frac{u_{i+1} - u_i}{\Delta x_1}\Delta t_1 a_n = u_i \tag{32}$$

$$a_n\left(1 + \frac{a_{i+1} - a_i}{\Delta x_1}\Delta t_1\right) - \frac{a_{i+1} - a_i}{\Delta x_1}\Delta t_1 u_n = a_i \tag{33}$$

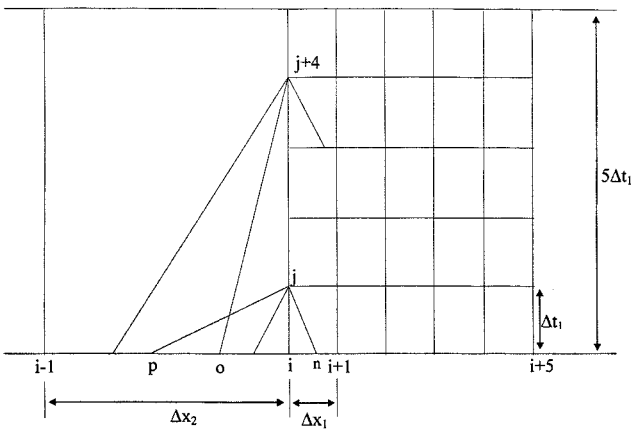

Figure 3. Boundary between fine and coarse meshes.

The solution for u_o depends on the direction of fluid flow.

For $\lambda_o > 0$ then

$$u_o = \frac{u_i}{\left(1 + \frac{u_i - u_{i-1}}{\Delta x_2} 4\Delta t_1\right)} \tag{34}$$

For $\lambda_o < 0$

$$u_o = \frac{u_i}{\left(1 + \frac{u_{i+1} - u_i}{\Delta x_1} \Delta t_1\right)} \tag{35}$$

The locations of x_o, x_p, and x_n can now be obtained directly from Eqs. 27–29 by substituting the calculated values for u_p, a_p, u_n, a_n, and u_o from the above equations. The values of P and T at the three initial points are then calculated using linear interpolation, and the corresponding density ρ and speed of sound a are obtained by performing an isothermal flash.

All the initial point flow variables are now available to compute the flow conditions at the solution point j. For the positive compatibility, it is

$$P_j - P_p + (\rho a)_p (u_j - u_p) = (\psi + a\beta)_p 4\Delta t_1 = K_1 \tag{36}$$

while for the negative compatibility, it is

$$P_j - P_n - (\rho a)_n (u_j - u_n) = (\psi - a\beta)_n \Delta t_1 = K_2 \tag{37}$$

Furthermore, the pathline compatibility for $\lambda_0 > 0$ is

$$P_j - P_o - (a^2)_o (\rho_j - \rho_o) = \psi_o 4\Delta t_1 \tag{38}$$

and the pathline compatibility for $\lambda_o < 0$ is

$$P_j - P_o - (a^2)_o (\rho_j - \rho_o) = \psi_o \Delta t_1 \tag{39}$$

Solving Eqs. 36 and 37 simultaneously for u_j one can write

$$u_j = \frac{K_1 - K_2 + (\rho a)_p u_p + (\rho a)_n u_n + P_p - P_n}{(\rho a)_n + (\rho a)_p} \tag{40}$$

The pressure may be calculated either from Eq. 36 or Eq. 37. The density at the solution point can now be obtained from the pathline compatibility. For $\lambda_o > 0$

$$\rho_j = \frac{(P_j - P_o) + a_o^2 \rho_0 - \psi_o 4\Delta t_1}{a_o^2} \tag{41}$$

The above procedures, also called the predictor steps, produce first estimates of the various flow parameters. Better estimations for these variables are obtained using an iterative procedure known as the corrector steps (Zucrow and Hoffman, 1976).

Table 1. Piper-Alpha to MCP-01 Pipeline and Isle of Grain Test Data*

		Isle of Grain	
	Piper Alpha	Test P40	Test P42
Pipeline length, L (km)	54	0.1	0.1
Inner dia., D (m)	0.419	0.15	0.15
Initial pres., P_{in} (bar)	117	21.6	11.3
Initial temp., T_{in} (K)	283	290.95	293.15
Heat-transfer coeff. U_h ($W/m^2 \cdot K$)	5.0 (Chen et al., 1992)	100 (Chen, 1993)	100
Pipe roughness factor (mm)	0.05	0.05	0.05
Ambient temp., T_∞ (K)	283	292.25	291.75

*Piper Alpha inventory (molar %); CH_4 (73.6), C_2H_6 (13.4), C_3H_8 (7.4), i-C_4H_{10} (0.4), n-C_4H_{10} (1.0), i-C_5H_{12} (0.08), n-C_5H_{12} (0.07), n-C_6H_{14} (0.02), N_2 (4.03). Isle of Grain inventory (molar %); C_3H_8 (95), n-C_4H_{10} (5).

Case Study

For obvious reasons, the amount of experimental data available relating to FBR is very scarce. The limited data reported are mainly confined to short (ca. 100 m) pipelines of small diameter (ca. 0.1 m) containing single component fluids. Following an extensive literature search, two sets of field data were identified, which are suitable for modeling purposes. The first set includes the intact end pressure data recorded during FBR of a long gas line, containing mainly methane connecting the Piper Alpha and MCP-01 platforms (Chen, 1993). The other set contains field data related to a series of pipeline depressurization tests carried out by Shell and British Petroleum on the Isle of Grain (Richardson and Saville, 1996). In these tests, extensively instrumented pipelines containing commercial liquefied petroleum gas (LPG) and incorporating pressure transducers and thermocouples were used. Inventory and holdup were also recorded using load-cells and neutron back scattering. Table 1 shows the prevailing experimental conditions, as well as the fluid compositions for the above cases.

Results and Discussion

Optimization of CNGS-MOC; effect of using a second-order or curved characteristic on the simulation accuracy and on CPU time

Figure 4 demonstrates the effect of using second-order characteristics on the CPU time when simulating FBR (see Table 1). The data show the variation of predicted release rate with time over the first 450 s following FBR using different numerical discretization techniques. All simulations were performed on a DEC Alpha server 8400 5/440. Curve A shows the results using a simple grid system (SGS) with a uniform Δx of only 10 m. This calculation is used as a reference for accuracy as it uses the finest grid system compared to the other simulations, and, hence, errors introduced as a result of numerical discretization are minimized. Curve B shows the results using the second-order (curved characteristics) solution for CNGS with a coarse grid Δx of 500 m. Curve C shows the CNGS results for the second-order solution with Δx of 250 m and, finally, curve D shows the first-order (linear approximation of characteristics) CNGS solution with Δx of 250 m. From these calculations, it is clear that the first-

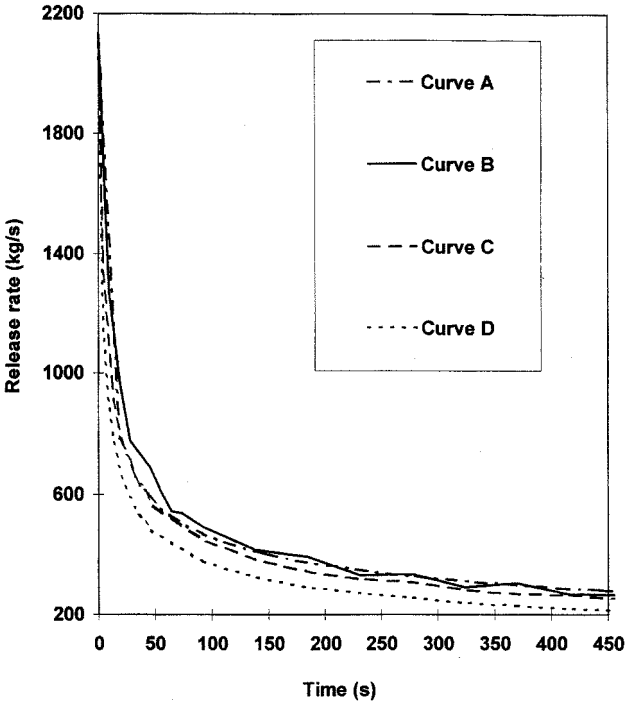

Figure 4. Piper Alpha: MCP line release rate profiles for different grid settings.

Curve A: First-order simple grid system (SGS), $\Delta x = 10$ m, CPU time = 250 h; Curve B: Second-order (CNGS-MOC), $\Delta x = 500$ m, CPU time = 3.75 h; Curve C: Second-order (CNGS-MOC), $\Delta x = 250$ m, CPU time = 12.2 h; Curve D: First-order (CNGS-MOC), $\Delta x = 250$ m, CPU time = 12.1 h.

order CNGS solution (curve D) consistently underestimates the release rate, whereas both second-order solutions produce good agreements. For the second-order solutions (curves B and C), an increase in Δx does not lead to an appreciable loss of accuracy, but the reduction of the CPU time is significant (cf. 12.2 h with 3.7 h). It is noteworthy that the use of the second-order characteristics in conjunction with the CNGS results in approximately 75 fold reduction (cf. 250 h; curve A with 3.75 h curve B) in CPU time. Based on the above, the second-order CNGS with a grid spacing of 500 m is chosen for the remaining of the validation tests.

Picard and Bishnoi (1989) reported diverging oscillations in pressure and density values with rapid termination of their FBR simulation when using a first-order method of characteristics. The authors were thus unable to report any data beyond the first few seconds of the modeling of a hypothetical break to a sour gas pipeline. The investigations show that this is mainly a consequence of the following:

(1) Use of linear interpolation for calculating bulk mixture density at intermediate points along the grid system. This presupposes a linear variation of fluid density with distance along the pipeline, thus giving rise to escalating errors. These errors become exacerbated in the case of two-phase mixtures particularly in the vicinity of the rupture plane. This problem is avoided by directly obtaining the fluid density from the EoS via an isothermal flash calculation at the specified pressure.

(2) The abrupt change in the speed of sound on crossing the gas/liquid interface means that if the characteristic lines

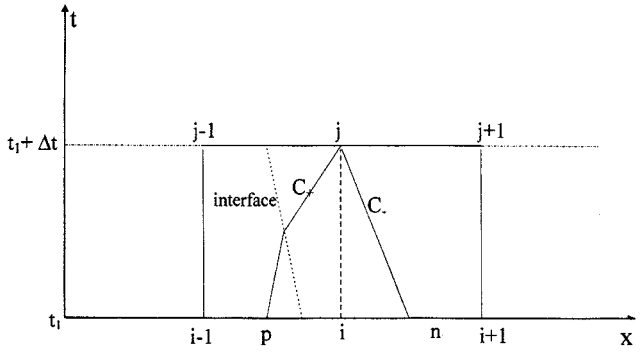

Figure 5. Refraction of characteristic lines at the single-phase/two-phase interface.

were to cross such an interface, significant refraction would occur. Figure 5 shows this type of phenomenon. To avoid instability, a substantially smaller value of Δt compared to that dictated by the CFL stability criterion is required. Experience has shown that a typical Δt value required in order to avoid instability is approximately 10% of the maximum value dictated by the CFL stability criterion.

Interestingly, it is found that even such a significant reduction in Δt does not result in an appreciable increase in the CPU time. This is primarily a consequence of the smaller number of iterations required in the corrector step in order to reach a solution.

Validation of the CNGS-MOC

Figure 6 shows the measured intact end pressure/time history following the FBR of Piper Alpha to MCP-01 subsea

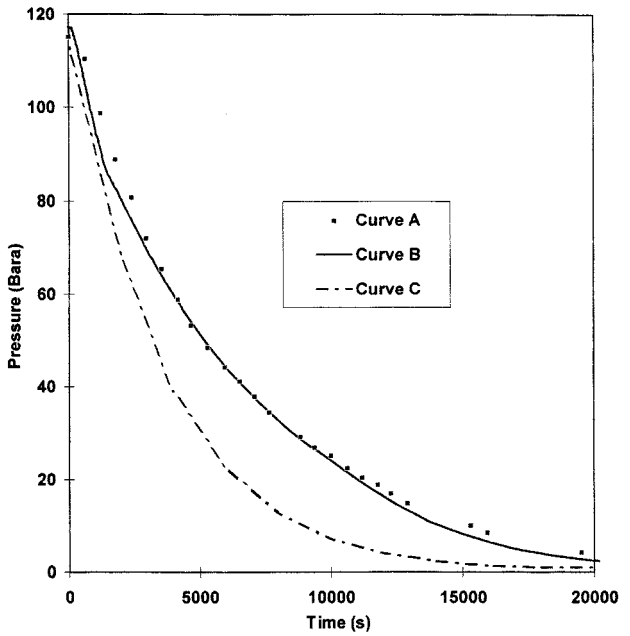

Figure 6. Intact end pressure vs. time profiles for Piper Alpha-MCP pipeline.

Curve A: Field data; Curve B: CNGS-MOC, CPU time = 6 days; Curve C: CNGS-MOC ideal gas, CPU time = 1.5 min.

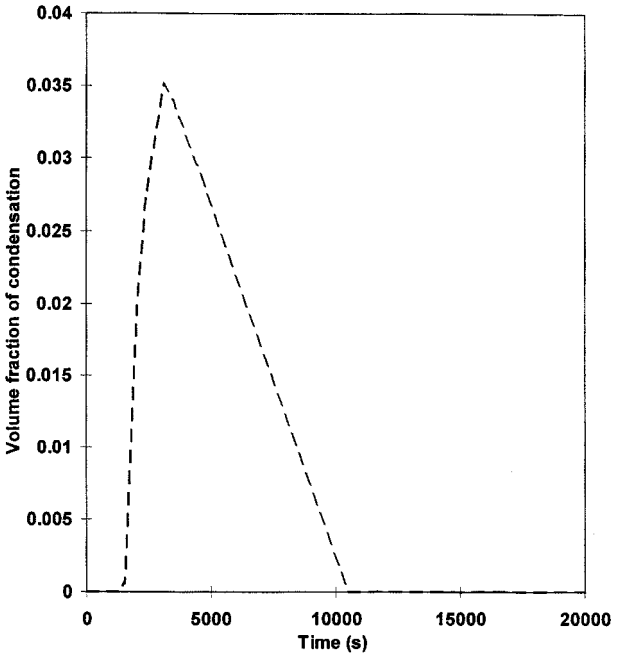

Figure 7. Condensation volume fraction at closed end for Piper Alpha-MCP line.

line. Curve A shows measured data, whereas curve B shows the predictions using the second-order CNGS-MOC, as described above. This is the first time that the entire release process has been simulated using a two-phase MOC model. Theory and experiment are in excellent agreement. Curve C shows the corresponding data generated using first-order characteristics in conjunction with the ideal gas assumption, CNGS-ideal as reported in our previous publication (Mahgerefteh et al., 1997). The discrepancy between ideal gas prediction and field data (curve A) demonstrates the importance of taking into account real fluid behavior when requiring accurate predictions.

The results for CNGS-MOC (curve B) show a slight deflection at about 1500 s. This corresponds to the onset of condensation at the closed end as indicated in Figure 7. These data show the variation of volume fraction of condensate with time at the closed end. The maximum liquid volume fraction is ca. 0.034 corresponding to a liquid mass fraction of about 15%. As the pipeline continues to depressurize, less inventory stays in the liquid phase and at about 10,000 s following FBR the closed end is exposed to gas only.

FBR experiments using LPG at the Isle of Grain

Figure 8 shows predictions for the open- and closed-end pressure-time histories for the LPG mixture, as compared to experimental data. Curves A and B show the measured data, whereas curves C and D represent the corresponding simulated data using CNGS-MOC. The extremely rapid initial decrease in pressure is due to an almost instantaneous change of phase from compressed liquid propane to a flashing two-phase mixture. The subsequent slight undershoot measured in pressure (curves A and B) is probably attributed to nonequilibrium effects such as delayed bubble nucleation, and possibly due to the reflection of expansion waves in the compressed liquid off the closed end of the pipe. The theoretical predictions represented by curves C and D are in fair agreement with the experimental data. Nevertheless, since immediate transition to the saturation conditions, is assumed one is unable to predict the initial undershoot due to the transition from liquid to two-phase flow. The finite discrepancies between theory and experiment may be attributed to a number of factors including the uncertainty associated with the measurement of pressure, the inaccuracies associated with the prediction of VLE data, the uncertainty in the selected pipe roughness, as well as the lack of accurate information on the fluid composition. The fluid composition chosen in this study is an approximate one for commercial LPG.

It is noteworthy that the measured data in Figure 8, as well as those presented in Figures 9–12 exhibit finite oscillations, although none of the simulations reviewed in this study, including ours, exhibit such behavior. It is strongly believed that this is a consequence of ignoring fluid-structure interaction (Lawooij and Tijsselling, 1990; Stittgen and Zielke, 1990) in the modeling. This is essentially a dynamic phenomenon, with the interaction being caused by dynamic forces which act conversely on fluid and pipe.

The simulations consider only rupture in straight, horizontal well-anchored pipelines in which the fluid compressibility is by far smaller than the pipe wall elasticity. Fluid-structure interaction can effectively be ignored.

Figure 9 shows the measured (curves A and B) and predicted temperature profiles (curves C and D) at the open and closed pipeline ends for test run P40. The predicted tempera-

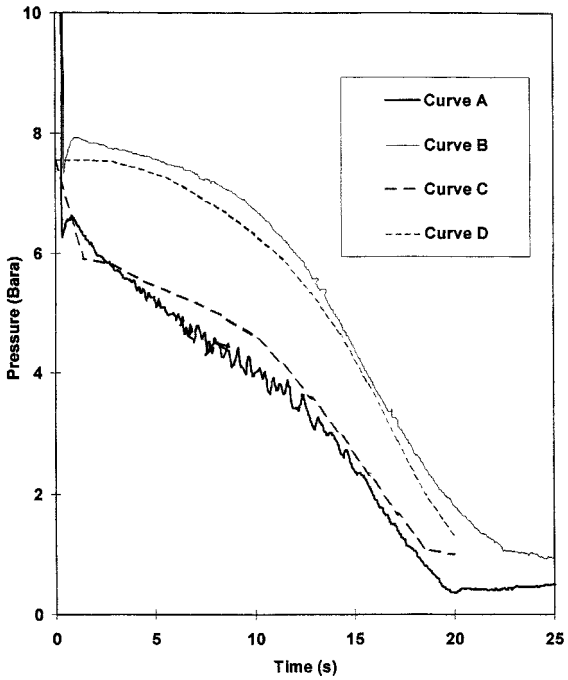

Figure 8. Pressure-time profiles at closed and open ends for the P40 test (LPG).

Curve A: Field data (open end); Curve B: Field data (closed end); Curve C: Open end, CNGS-MOC; Curve D: Closed end, CNGS-MOC.

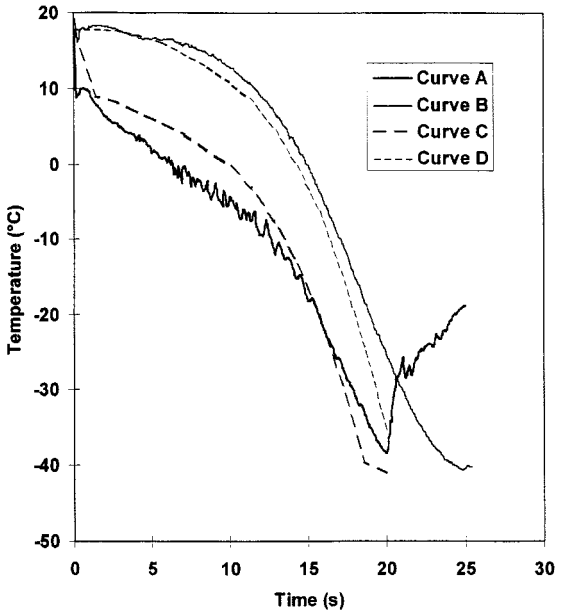

Figure 9. Temperature-time profiles at the open and closed ends for the P40 test (LPG).

Curve A: Field data (open end); Curve B: Field data (closed end); Curve C: CNGS-MOC (open end); Curve D: CNGS-MOC (closed end).

ture profiles show similar trends with those observed above for the pressure profiles when compared to experimental data. The open-end predictions are slightly higher, whereas the closed-end predictions are slightly lower than measured data. The maximum discrepancy is about 5°C. A significant and

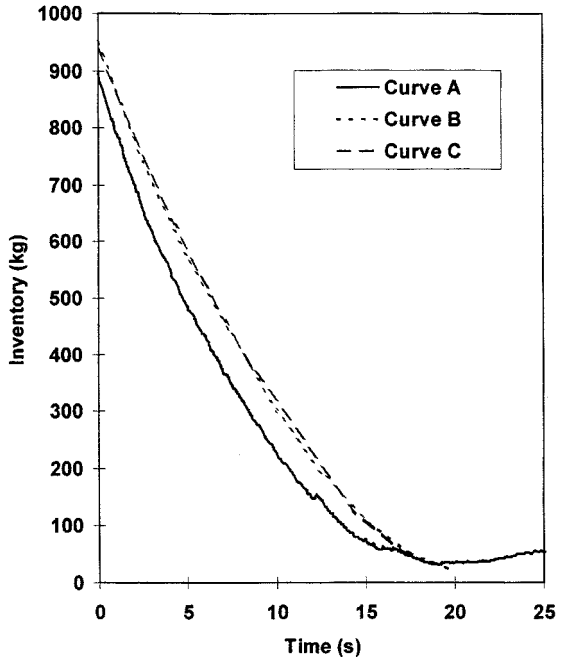

Figure 10. Total line inventory predictions for the P40 test (LPG).

Curve A: Field data; Curve B: META-HEM; Curve C: CNGS-MOC.

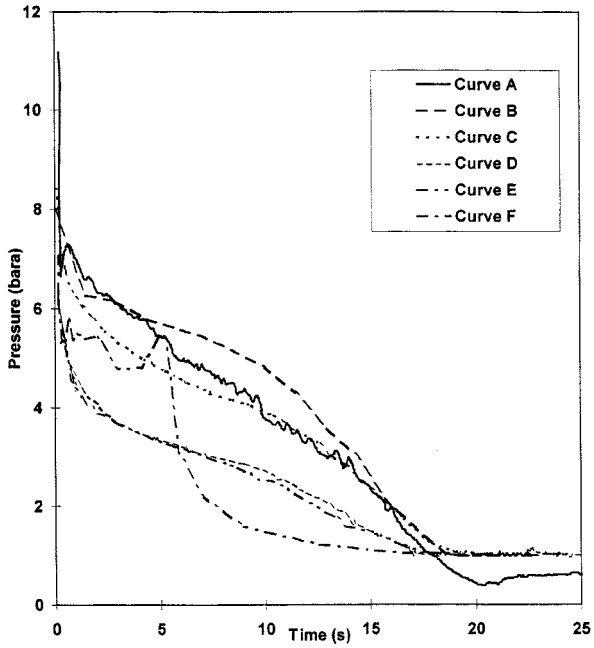

Figure 11. Pressure-time profiles at the open end for the P42 test (LPG).

Curve A: Field data; Curve B: CNGS-MOC; Curve C: META-HEM; Curve D: MSM-CS; Curve E: Blowdown; Curve F: Plac.

rapid increase in the measured temperature at the open end (curve A) can be observed towards the end of the depressurization process. This rise corresponds to the cessation of

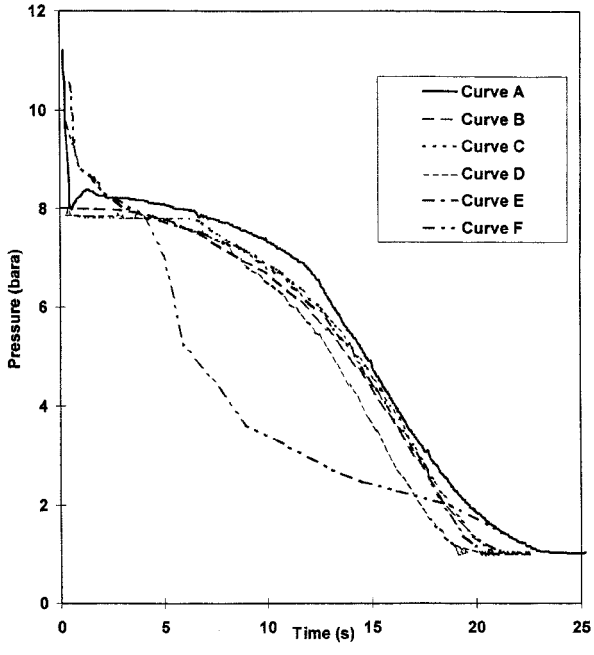

Figure 12. Pressure-time profile predictions at the closed end for the P42 test (LPG).

Curve A: Field data; Curve B: CNGS-MOC; Curve C: META-HEM; Curve D: MSM-CS; Curve E: BLOWDOWN; Curve F: PLAC.

two-phase flow with the subsequent onset of gas-phase flow at the rupture plane, and is probably a reflection of different heat-transfer rates from the wall to the fluid. This trend cannot be reproduced with the model as a constant heat-transfer coefficient is employed. The slight leveling of the temperature immediately before its subsequent rise corresponds to the moment when the flow at the rupture plane ceases to be choked.

Figure 10 shows a comparison for the total line inventory during depressurization for the test run P40. Curve A shows the load cell values, whereas curves B and C show the predictions using META-HEM (Chen et al., 1993, 1995; Chen, 1995) and the CNGS-MOC model, respectively. META-HEM is a homogeneous equilibrium model that uses a FDM to resolve the Euler equations. Both models slightly overestimate line inventory, but give very similar results.

In Figure 11, experimental data (curve A) and theoretical predictions are shown for the open-end pressure for the P42 case using CNGS (curve B) and other models including META-HEM (curve C), MSM-CS (curve D), BLOWDOWN (curve E), and PLAC (curve F) for the LPG mixture. In Figure 12, the corresponding predictions at the closed end are shown. The BLOWDOWN model was developed by Richardson and Saville (1991), the MSM model by Chen (1993), and PLAC by Hall et al. (1993). The BLOWDOWN simulation (curve E) for pipelines is based on quasi-steady-state, equilibrium, and homogeneous two-phase flow assumptions. The MSM-CS model (curve D) takes into account the slip velocity between the two phases, and, thus, incorporates the relevant hydrodynamic constitutive relations that accompany this effect. As a result, two momentum equations, one for each phase, are solved instead of just one in META-HEM. The MSM is based on the same solution techniques as META-HEM. PLAC (curve F) is an extension of the nuclear reactor safety code TRAC in that it incorporates a flash calculation package MULTIFLASH to predict VLE data for hydrocarbon mixtures. In addition, the original critical flow boundary condition in TRAC is replaced by a homogeneous frozen flow model that allows different temperatures for each of the two phases, and, thus, permits thermal nonequilibrium since two energy equations are solved for each phase. This creates a dilemma as to which temperature should be used for the equilibrium phase behavior, an inevitable problem in determining the phase behavior of multicomponent mixtures.

From Figure 11 it is apparent that the best predictions are obtained from CNGS-MOC and META-HEM. BLOWDOWN substantially underestimates open-end pressure because of the quasi-steady flow assumption and MSM-CS gives almost the same predictions as BLOWDOWN. It is surprising that the former cannot provide a better prediction of the pressure profile at the open end. This could be due to the use of unrealistic hydrodynamic constitutive relations. Another possible reason is the inaccuracy in predicting the wave propagation velocities.

PLAC also gives rise to poor predictions. It predicts a large drop in pressure of at least 2 bara at about 5 s after rupture and continues to drop thereafter. One reason for this discrepancy might be due to the fact that no actual flash calculations are performed to determine fluid properties during the depressurization. Depressurization profiles for mixtures such as LPG are especially sensitive to accurate thermodynamic prediction due to the *narrow* phase envelop involved. In PLAC, fluid physical properties are calculated at a given pressure and temperature in a cell by interpolation from look-up tables generated using a phase equilibrium package before transient flow calculations begin.

Based on the comparison of total line inventory prediction for test P42, Chen (1993) showed that the initial inventory from PLAC starts at a much lower value (695 kg) than the experimental (970 kg), and drops to less than 20% within 5 seconds. The considerable under-estimation can be attributed to two possible reasons. Firstly, too much gas formation is predicted in the pipeline by PLAC resulting in lower line inventory prediction. Hall et al. (1993) take the initial state of the fluid as 80% liquid which means that in PLAC transient flow calculations start at a point that is already quite well into two-phase flow as opposed to near the saturation point. In the CNGS-MOC, calculations start at the saturation point producing good initial agreement. A second reason could be due to overestimation of the release rate by the homogeneous frozen critical flow boundary condition.

Figure 12 shows the same data as those presented in Figure 11, but for the closed end. CNGS-MOC, META-HEM, and BLOWDOWN give very similar predictions with MSM doing less well and PLAC performing very poorly. As for the open-end pressure predictions, PLAC shows a very sharp drop in pressure at ca. 5 s and continues to drop at a much faster rate than the other models thereafter. Once again, the CNGS-MOC provides relatively good predictions of the conditions following FBR.

Conclusions

In this article, the development of an efficient numerical simulation (CNGS-MOC) is described that is based on the method of characteristics for simulating the variations in fluid dynamics following full bore rupture of long pipelines containing high-pressure two-phase hydrocarbon mixtures. The long CPU time has been largely addressed, and this has been synonymous so far with such types of simulations by using curved characteristics in conjunction with a compound nested grid system, as well as setting up and solving a system of simultaneous equations. As opposed to the commonly used linear characteristics, curved characteristics are found to afford the use of much larger discretization grids, while at the same time improve the global accuracy. Also, the number of iterations involved in arriving at a solution in the corrector step is significantly reduced.

It is expected that the application of curved characteristics is particularly pertinent in the case of two-phase flows, especially near the rupture plane where the variations in fluid properties are highly nonlinear. Instability problems are overcome, which invariably result in premature termination of such types of simulations by obtaining the relevant fluid properties at intermediate points along the grids from the equation of state directly. This is an improvement over previous work, where an interpolation was used which relies on a linear variation of fluid properties in between grid points.

Extensive comparison with experimental data revealed that the model produces reliable results in terms of predicting various parameters including pressure, temperature, and total line inventory variations with time following FBR. It also

compares very favorably with META-HEM, while, in comparison, other models such as BLOWDOWN, MSM-CS, and PLAC perform surprisingly poorly. The success of the CNGS-MOC in simulating FBR is indicative of the applicability of HEM in such types of processes.

In conclusion, this work shows that FBR can be simulated effectively using the method of characteristics in conjunction with the homogeneous equilibrium model, given an accurate thermodynamic and phase behavior model. Apart from its accuracy, a particularly attractive feature of MOC is the ease with which it may be used for simulating the dynamic response of emergency shutdown valves following FBR by simple implementation of the appropriate boundary conditions at the location of the valves.

So far, all of the existing numerical mathematical treatments for simulating FBR require the use of powerful workstations. Given the current rapid pace in computer processing speeds, it is believed that the CNGS-MOC described in this study offers the best chance for carrying out such types of simulations accurately on personal computers in reasonably practical time scales.

Literature Cited

Assael, M. J., J. P. Martin Trusler, and T. Tsolakis, *Thermophysical Properties of Fluids*, Imperial College Press, London (1996).

Bendiksen, K. H., D. Malnes, R. Moe, and S. Nuland, ''The Dynamic Two-Fluid Model OLGA: Theory and Application,'' *SPE Production Eng.*, 6, 171 (1991).

Bisgaard, C., H. H. Sorensen, and S. Spangenberg, ''A Finite Element Method for Transient Compressible Flow in Pipelines,'' *Int. J. Num. Meth. Fluids*, **7**, 291 (1987).

Bond, J., ''IChemE Accidents Database,'' IChemE, Rugby, U.K. (1996).

Chen, C. R., S. M. Richardson, and G. Saville, ''Numerical Simulation of Full-bore Ruptures of Pipelines Containing Perfect Gases,'' *Trans. Inst. Chem. Eng. Part B*, **70**, 59 (1992).

Chen, J. R., ''Modelling of Transient Flow in Pipeline Blowdown Problems,'' PhD Thesis, Univ. of London, Imperial College (1993).

Chen, C. R., S. M. Richardson, and G. Saville, ''A Simplified Numerical Method for Transient Two-phase Flow,'' *Trans. IChem. E.*, **71A**, 304 (1993).

Chen, C. R., S. M. Richardson, and G. Saville, ''Modelling of Two-phase Blowdown from Pipelines: I. A Hyperbolic Model Based on Vibrational Principles,'' *Chem. Eng. Sci.*, **50**, 695 (1995).

Chen, C. R., S. M. Richardson, and G. Saville, ''Modelling of Two-Phase Blowdown from Pipelines: II. A Simplified Numerical Method for Multi-component Mixtures,'' *Chem. Eng. Sci.*, **50**, 2173 (1995).

Courant, R., K. O. Friedrichs, and H. Lewy, ''Uberdie Partiellen Differenzialgleichungen der Mathematisehen, Physik,'' *Mathematische Annalen*, **100**, 32 (1926).

Cullen, W. D., ''The Public Inquiry into the Piper Alpha Disaster,'' Dept. of Energy, HMSO, London (1990).

Flatt, R., ''A Singly-iterative Second Order Method of Characteristics for Unsteady Compressible One Dimensional Flows,'' *Comm. in Appl. Num. Meth.*, **1**, 269 (1985).

Flatt, R., ''Unsteady Compressible Flow in Long Pipelines Following a Rupture,'' *Int. J. Num. Meth. Fluids*, **6**, 83 (1986).

Groves, T. K., P. R. Bishnoi, and J. M. E. Wallbridge, ''Decompression Wave Velocities in Natural Gases in Pipelines,'' *Can. J. Chem. Eng.*, **56**, 664 (1978).

Hall, A. R. W., G. R. Butcher, and C. E. The, ''Transient Simulation of Two-phase Hydrocarbon Flows in Pipelines,'' *Proc. Euro. Two-Phase Flow Group Meeting*, Hannover, Germany (June 6–10, 1993).

HMSO, ''The Offshore Installations Emergency Pipeline Valve Regulations, Statutory Instruments,'' Health and Safety Executive, Bootle, U.K. (1989).

Lawooij, C. S. W., and A. S. Tijsselling, ''Waterhammer with Fluid-Structure Interaction,'' *App. Scient. Res.*, **47**, 273 (1990).

Lang, E., ''Gas Flow in Pipelines Following a Rupture Computed by a Spectral Method,'' *J. Appl. Math. and Physics (ZAMP)*, **42**, 183 (1991).

Lyczkowski, R. W., D. Gidaspow, C. W. Solbrig, and E. D. Hughes, ''Characteristics and Stability Analysis of Transient One-dimensional Two-Phase Flow Equations and Their Finite Difference Approximations,'' *Nucl. Sci. Eng.*, **66**, 378 (1978a).

Lyczkowski, R. W., R. A. Grimesey, and C. W. Solbrig, ''Pipe Blowdown Analyses Using Explicit Numerical Schemes,'' *AIChE Symp. Ser.*, **174**, 129 (1978b).

Mahgerefteh, H., P. Saha, and I. G. Economou, ''A Study of the Dynamic Response of Emergency Shutdown Valves Following Full Bore Rupture of Gas Pipelines,'' *Trans. Inst. Chem. Eng., Part B*, **75**, 201 (1997).

Mahgerefteh, H., P. Saha, and I. G. Economou, ''Control Valves for Pipe Rupture,'' *The Chem. Engineer*, **666**, 26 (1998).

Massey, B. S., *Mechanics of Fluids*, Van Nostrand Reinhold, Wokingham, U.K. (1983).

Michelsen, M. L., ''The Isothermal Flash Problem: I. Stability,'' *Fluid Phase Equil.*, **9**, 1 (1982a).

Michelsen, M. L., ''The Isothermal Flash Problem: II. Phase-Split Calculation,'' *Fluid Phase Equil.*, **9**, 21 (1982b).

Michelsen, M. L., ''Multi-Phase Isenthalpic and Isentropic Flash Algorithms,'' *Fluid Phase Equil.*, **33**, 13 (1987).

Olorunmaiye, J. A., and N. E. Imide, ''Computation of Natural Gas Pipeline Rupture Problems Using the Method of Characteristics,'' *J. Hazardous Mat.*, **34**, 81 (1993).

Peng, D. Y., and D. B. Robinson, ''A New Two-constant Equation of State,'' *Ind. Eng. Chem. Fund.*, **15**, 59 (1976).

Picard, D. J., and P. R. Bishnoi, ''The Importance of Real-fluid Behaviour in Predicting Release Rates Resulting from High Pressure Sour-gas Pipeline Ruptures,'' *Can. J. Chem. Eng.*, **67**, 3 (1989).

Picard, D. J., and P. R. Bishnoi, ''The Importance of Real-fluid Behaviour and Nonisentropic Effects in Modelling Decompression Characteristics of Pipeline Fluids for Application in Ductile Fracture Propagation Analysis,'' *Can. J. Chem. Eng.*, **66**, 3 (1988).

Press, H. W., S. A. Teukolsky, W. T. Vetterling, and B. P. Flannery, *Numerical Recipes in Fortran*, 2nd ed., Cambridge Univ. Press, Cambridge (1994).

Richardson, S. M., and G. Saville, ''Blowdown of Pipelines,'' paper SPE 23070, Society of Petroleum Engineers Offshore Europe 91, Aberdeen, U.K., 369 (1991).

Richardson, S. M., and G. Saville, ''Blowdown of LPG Pipelines,'' *Trans. Inst. Chem. Eng. Part B*, **74**, 235 (1996).

Saha, P., ''Modelling the Dynamic Response of Emergency Shutdown Valves Following Full Bore Rupture of Long Pipelines,'' PhD Thesis, Univ. College London (1997).

Stittgen, M., and W. Zielke, ''Fluid Structure Interactions in Flexible Curved Pipes,'' *Proc. of 6th Int. Conf. on Pressure Surges*, A. R. D. Thorley, ed., BHRA, 101 (1990).

Weiss, M. H., K. K. Botros, and W. M. Jungowski, ''Simple Method Predicts Gas Blowdown Time,'' *Oil and Gas. J.*, 12, 55 (1988).

Wood, D. J., and J. E. Funk, ''A Boundary Layer Theory for Transient Viscous Losses in Turbulent Flow,'' *ASME J. Basic Eng.*, **92**, 865 (1970).

Zucrow, M. J., and J. D. Hoffman, *Gas Dynamics*, Vols. I and II, Wiley, New York (1976).

Manuscript received Dec. 7, 1998, and revision received Mar. 29, 1999.